DOI:10.1158/0008-5472.CAN-05-3294

Cancer Research

Subtractive Transcriptomics: Establishing Polarity Drives *In vitro* Human Endothelial Morphogenesis

David A. Glesne, Wen Zhang, Suneeta Mandava, et al.

Cancer Res 2006;66:4030-4040. Published online April 17, 2006.

DOI:10.1158/0008-5472.CAN-05-3294

Research Article

Subtractive Transcriptomics: Establishing Polarity Drives *In vitro* Human Endothelial Morphogenesis

David A. Glesne, Wen Zhang, Suneeta Mandava, Lyann Ursos, Margaret E. Buell, Lee Makowski, and Diane J. Rodi

Biosciences Division, Argonne National Laboratory, Argonne, Illinois

Abstract

Although investigations of mature normal and tumor-derived capillaries have resulted in characterization of these structures at the phenotypic level, less is known regarding the initial molecular cues for cellular assembly of endothelial cells into human capillaries. Here, we employ a novel combination of microenvironmental manipulation and microarray data filtration over narrowly delineated temporal data series to identify the morphogenesis component apart from the proliferation component, as pooled human microvascular-derived endothelial cells are induced to form capillary-like structures *in vitro* in a murine tumor-derived matrix. The 217 morphogenesis-specific genes identified using this subtractive transcriptomics approach are mostly independent of the angiogenic proteins currently used as therapeutic targets for aberrant angiogenesis. Quantitative real-time PCR was used to validate 20% of these transcripts. Immunofluorescent analysis of proliferating and tube-forming cells validates at the protein level the morphogenesis-specific expression pattern of 16 of the 217 gene products identified. The transcripts that are selectively up-regulated in tube-forming endothelial cells reveal a temporal expression pattern of genes primarily associated with intracellular trafficking, guided migration, cytoskeletal reorganization, cellular adhesion, and proliferation inhibition. These data show that a sequential up-regulation of genes that establish and maintain polarity occurs during migration and morphogenesis of *in vitro* human endothelial cells undergoing tubulogenesis; some of which may well be effective as novel antiangiogenic drug targets. (Cancer Res 2006; 66(8): 4030-40)

Introduction

The growth of new capillaries from preexisting networks (angiogenesis) is an essential component of embryogenesis and reinitiates in the adult animal during tissue growth and repair processes, such as wound healing and the menstrual cycle. Misregulation of this tightly controlled process has been shown in multiple pathologic conditions in humans, including retinopathy, rheumatoid arthritis, and tumor progression, in which it is instrumental in tumor invasion and metastasis. It is driven by a highly complex and orchestrated genetic program in which endothelial cell proliferation combines with branching morphogenesis, the latter of which requires major changes in both functional and spatial cellular organization. Little is known about the proteins regulating changes in cell shape, long-range migration, and communication necessary for capillary formation that are associated with actual morphogenesis. These proteins are far more likely to be specific to angiogenesis than those involved in endothelial cell proliferation, which currently represent the majority of drug targets of angiogenic-modulating drug candidates. Consequently, a method for identifying morphogenesis-selective proteins is critical to further development of antiangiogenic therapies.

The molecular dissection of complex cellular processes is one of the major challenges in postgenomics biology. Several *in vitro* models have been developed over the past few years, which have served as high-throughput primary assays to test both proangiogenic and antiangiogenic agents (see the pro and con discussion of these models in ref. 1). Previous microarray analyses of collagen- or Matrigel-induced tube formation *in vitro* by other groups (2–6) have focused on either proliferation-associated transcripts or used a single time point, plus/minus approach, followed by bioinformatic dissection of statistically high-scoring (i.e., highly expressed) transcripts. Although these studies have provided valuable insight into characteristics that define the phenotype of mature endothelial cells, absent from our knowledge is much of the temporally regulated information inherent to a dynamic process, such as vascularization, and the identification of proteins that are expressed transiently and/or weakly that may be central to the initiation of angiogenesis.

To identify proteins potentially involved strictly in the regulation of endothelial cell "morphogenesis" as opposed to "proliferation," gene expression in pooled human microvascular endothelial cells (HMVEC) undergoing the two processes *in vitro* were contrasted and compared. When cultured on gelatin-coated plastic, these cell explants undergo proliferation. Alternately, when seeded at an appropriate density on a gel composed of extracted basement membrane derived from mouse Engelbreth-Holm-Swarm sarcoma (Matrigel), the endothelial cells migrate into the matrix and proceed to form capillary-like lumen-containing structures (7). It has been shown that malignant tumor cells recruit vasculature through both the production and the secretion of growth factors and interaction with locally activated host microenvironment. Tumors activate angiogenesis in a polymorphic manner, with a wide variation in the diameter and density of the formed vessels (see ref. 8 as an example) possibly due to the variation seen in the class and level of growth factors up-regulated as well as the wide variation in local environmental factors present. The Matrigel-driven tubulogenesis model was chosen for this preliminary array analysis to reduce nonendothelial transcript background and to provide initial drug target candidates specific for morphogenesis that could be followed up in later *in vivo* studies. Comparison of the two temporal processes provides the ability to separate the

Note: Supplementary data for this article are available at Cancer Research Online (http://cancerres.aacrjournals.org/).

Requests for reprints: Diane J. Rodi, Biosciences Division, Argonne National Laboratory, 9700 South Cass Avenue, Argonne, IL 60439. Phone: 630-252-3963; Fax: 630-252-5517; E-mail: drodi@anl.gov.

doi:10.1158/0008-5472.CAN-05-3294

DOI:10.1158/0008-5472.CAN-05-3294

proliferation phase of angiogenesis from early network formation in a simple *in vitro* model system and offers the opportunity to identify important proteins up-regulated early on in capillary morphogenesis yet not during the growth process.

Materials and Methods

Reagents and cell culture. Pooled, neonatal dermis HMVECs were obtained from Cascade Biologics, Inc. (Portland, OR) and maintained as recommended. Recombinant human vascular endothelial growth factor (rhuVEGF) was obtained from Alpha Diagnostics International (San Antonio, TX), Matrigel was from Becton Dickinson Co. (Franklin Lakes, NJ), and TRIzol reagent was from Invitrogen (Frederick, MD).

Formation of three-dimensional tubes on Matrigel. Subconfluent HMVECs at passage 5 to 7 were plated onto the Matrigel-coated dishes (with addition of purified rhuVEGF at 50 ng/mL to the medium and the Matrigel) at 2.25×10^4 cells/cm^2. Control plates of proliferating subconfluent cells were washed with PBS thrice and overlaid with medium supplemented with the same level of rhuVEGF. Tube formation was monitored via light and Nomarski differential interference contrast (DIC) microscopy. Before DIC microscopy, cells were fixed with 4% formaldehyde (EM grade, Electron Microscopy Sciences, Ft. Washington, PA). DIC microscopy was carried out on a Leica (Allendale, NJ) DMXRE microscope at sector 2 of the Advanced Photon Source at Argonne National Laboratory.

Electron microscopy. Cells grown on Matrigel-coated Permanox-coated chamber slides were fixed, treated with 1% uranyl acetate, dehydrated, and infiltrated with Spurr's resin/propylene oxide at room temperature. Samples were polymerized, serially cut at 90 nm, stained with uranyl acetate and lead citrate, and viewed under a FEI Tecnai F30st-STEM microscope (FEI Co., Eindhoven, the Netherlands) operated at 300 keV.

RNA isolation, quality assessment, and microarray analysis. Quality-control assessments were done at three different stages: before hybridization, during target preparation, and posthybridization. Total RNA was purified from TRIzol suspensions at five time points "each" for proliferating ("VEGF series") and tube-forming ("tube series") HMVECs according to manufacturer's instructions. RNA preparations were further purified using RNEasy MinElute Clean Up columns (Qiagen, Valencia, CA). RNA quality was defined as minimum required A_{260}/A_{280} and A_{260}/A_{230} ratios of 1.8. *In vitro* transcribed cRNA (15 μg) was used from each of the samples. Hybridization to Affymetrix (Santa Clara, CA) GeneChip Human Genome U133 (HG-U133A and HG-U133B) arrays was carried out by the Functional Genomics Facility at the University of Chicago. Hybridization quality was evaluated by examining the report file for housekeeping gene hybridization, spike control hybridization, percentage of genes called present, 3′ to 5′ ratio, and background and scale factor ratio and by dChip analysis for regional image contamination and/or sample contamination.

Data analysis and filtration and gene annotation. Chip data were analyzed with the Affymetrix GeneChip analysis software (version 3.2) and GeneSpring software (version 5.0.2, Silicon Genetics, Santa Clara, CA). Raw expression scores were normalized using GeneSpring's default Per Chip Per Gene method. Mathematically, a morphogenesis-selective transcript (MRSL) has a normalized expression value at any one tube series time point at least 2-fold greater than all of the normalized expression values in the proliferation series. To create this list, a series of filters were applied to the time series data in terms of fold change or expression levels of normalized data, and the intersection or union of the series of lists was obtained using Venn diagrams. A maximum normalized value of 1.0 for the proliferation series (to eliminate high scores) and a minimum normalized value of 1.0 for the tube formation series (to eliminate low scores) were then applied to this interim sequence list.

Gene mapping and chip annotation was accomplished by using the alignment tools of the ENSEMBL, University of California at Santa Cruz, and National Center for Biotechnology Information (NCBI) Human Genome browsers[1] using the individual 25-nucleotide oligonucleotide sequences. Sequences which did not lie within coding regions, were discarded. Functional annotations were carried out using publicly available databases.

Quantitative real-time PCR analysis. Quantitative real-time PCR (QRT-PCR) was done using the Brilliant QPCR Core Reagent kit (Stratagene, La Jolla, CA) with rRNA as a control. Gene expression was quantified using the comparative C_T method with 18S rRNA as reference (see ref. 9 for detailed methods). PrimerExpress software (ABI, Foster City, CA) was used to design primers and probes.[2] Reactions were run on a Stratagene Mx4000 Multiplex Quantitative PCR System in 96-well formats.

Immunofluorescence and visualization. HMVEC tube structures or proliferating HMVECs on 35-mm tissue culture plates coated with Matrigel and gelatin, respectively, were fixed, permeabilized, and incubated with 1:2,000 to 1:5,000 dilution of one of the following primary antibodies in 1% bovine serum albumin/PBS: rabbit anti–ephrin A1 (Zymed Laboratories, Inc., South San Francisco, CA), mouse anti-nestin (Chemicon International, Temecula, CA), and anti-ADAM19 (Novus Biologicals, Littleton, CO). The cells were then hybridized with a 1:200 dilution of secondary antibodies conjugated with either Alexa Fluor 488 or Alexa Fluor 555 (Molecular Probes, Eugene, OR) and with 4′,6-diamidino-2-phenylindole (DAPI) at a 1:100 dilution from the stock solution (30 g/mL; Polysciences, Inc., Warrington, PA). Cells were mounted using gelvatol (Monsanto, St. Louis, MO) in glycerol and imaged using a Zeiss (Thornwood, NJ) AxioCam microscope with AxioVision 3.1 digital imaging software. DAPI exposure times are 99 ms, whereas FITC channel exposure times ranged from 10.25 seconds for low-expressing proteins, such as nFATc2, to 3 to 4 seconds for higher-expressing proteins, such as ephrin A3.

Western blotting. Total cell protein was isolated by Matrisperse digestion according to the manufacturer's instructions (Becton Dickinson) followed by centrifugation, washing with PBS, and lysis in 1× Laemmli buffer [25 mmol/L Tris-HCl (pH 8.3), 250 mmol/L glycine, 0.1% SDS]. Proteins were separated by SDS-PAGE, transferred to Hybond-C membranes (Amersham Life Sciences, Piscataway, NJ), and blocked with 5% nonfat milk in PBS containing 0.05% Tween 20 with agitation. Tetranectin was visualized by incubation with primary unlabeled rabbit anti-tetranectin antibody (DAKO Corp., Carpinteria, CA) in blocking buffer followed by incubation with horseradish peroxidase–labeled anti-rabbit IgG cross-absorbed conjugates (Jackson Immunoresearch, West Grove, PA) and chemiluminescent detection using SuperSignal West Femto visualization reagents (Pierce Chemical, Rockford, IL).

Monte Carlo simulation of MRSL gene chromosomal location. Correlation coefficients and Monte Carlo simulations were carried out using the number of predicted genes per chromosome in the NCBI *Homo sapiens* Genome Build 35 version 1. The probability that two MRSL genes would be placed immediately adjacent to one another in a chromosome of n genes containing m MRSL genes was calculated by a Monte Carlo simulation using 10,000 trials, each trial consisting of the random placement of genes within a chromosome and tabulation of the number of times MRSL genes are placed as nearest neighbors.

Results

Morphologically, Matrigel-driven tubulogenesis occurs in two discrete phases: an early attachment, migration, and cord-like formation phase lasting up to 2 hours postplating involving significant process formation (Fig. 1*A* and *B*) followed by a reorganization and consolidation phase extending from 2 to 8 hours and later (Fig. 1*C*; ref. 10). Electron microscopy confirmed progressive vacuolation, increasing in both diameter and number per cell and leading to the formation of single cells containing a lumen of ~2 μm by 8 hours with the appearance of multicellular lumen of

[1] http://www.ensembl.org/Homo_sapiens/, http://www.genome.ucsc.edu/, and http://www.ncbi.nlm.nih.gov/genome/seq/HsBlast.html.

[2] For all primer/probe sequences used, see http://relic.bio.anl.gov/Glesne_etal2006_QRT_PCR_primer_probe_sequences.htm.

DOI:10.1158/0008-5472.CAN-05-3294

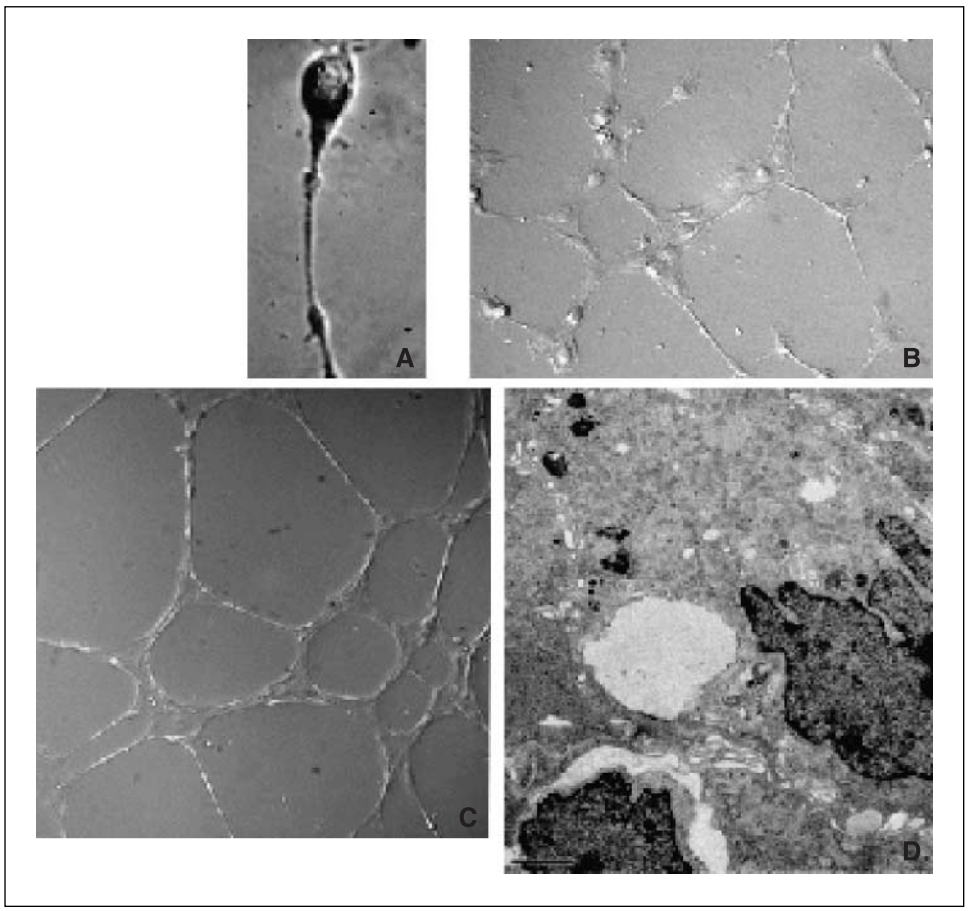

Figure 1. HMVEC tube morphogenesis during experimental period. HMVEC tube formation on Matrigel was monitored by light microscopy (*A* and *B*), DIC microscopy (*C*), and electron microscopy (*D*). *A,* a purposely underplated HMVEC on Matrigel as described in Materials and Methods. Magnification, ×400. HMVECs at 2 hours (*B*) and 8 hours (*C*) postplating under the standardized conditions indicated in Materials and Methods. Magnification, ×100. Vacuolation and lumen formation were monitored using electron microscopy, with multicellular structures with a single lumen of 3 to 4 μm across at 15 hours postplating (*D*). Bar, 2 μm.

3 to 4 μm in diameter by 15 hours (Fig. 1*D*). Studies carried out at lower cell density to slow tube formation show that the earliest morphologic change on attachment to matrix was the formation of long, thin actin-based processes between neighboring cells (Supplementary Fig. S1A; refs. 11, 12).

The microarray analysis was designed to observe early activities (5), including transient transcription factor up-regulation (3), with the first RNA samples isolated 30 minutes postplating. As internal controls for both the validity of the cell culture system as a model for tumor-induced angiogenesis and the subsequent microarray analyses, we analyzed the expression profiles of several transcripts known to be induced by VEGF within endothelial cells. High raw and normalized scores were noted in a time-dependent fashion for HEY1, HEY2, COX2, EGR3, and CXCR4 (Supplementary Fig. S2; refs. 4, 13–15). Serial induction of EGR1 mRNA was followed 1 hour later by up-regulation of tissue factor mRNA, an EGR1-responsive gene, in both time series, showing the utility of the chosen time points for distinguishing distinct expression phases within the system (Supplementary Fig. S3). Analysis of 203 known angiogenesis proteins in the array data set (defined by the MEDIC Breast Cancer Project as being relevant to the angiogenic process) showed that 109 (54%) were detectable in both proliferating and tube-forming cells, 50 (25%) were not detectable in either time series, 10 (5%) were detected only in the proliferating cell data set, and 34 (17%) were tube formation specific (Table 1, *top*; Supplementary Table S1). These data indicate that only about one-sixth of these sequences defined as angiogenic are associated solely with the morphogenesis aspect of the process.

The majority of microarray studies of endothelial cells have similarly identified transcripts associated with proliferation, not tubulogenesis, as shown by an exhaustive comparative analysis between this data set and previously published studies of endothelial cell gene expression patterns. Previous related microarray and/or cDNA studies showed significant overlap with transcripts up-regulated during the proliferation time series but included almost no MRSLs (2–6, 16–18), emphasizing the value of using temporal expression patterns during proliferation as a background control and examining the process at its earliest initiation in the identification of sequences associated strictly with morphogenesis. Analysis of the MRSL list in the context of endothelial cell specialization (19) and tumor angiogenesis (20, 21) indicated no obvious overlap of genes. This overall lack of concordance of our MRSL list with proteins previously identified as angiogenic/endothelial reflects the emphasis in previous studies placed on mature and/or proliferating endothelial cells, whereas the MRSL proteins identified here are more likely to be involved in regulating and coordinating nascent vasculature.

The multistep informatic filtering algorithm employed as described in Materials and Methods was designed to remove transcripts related primarily to proliferation, nonspecific attachment, or cytokine response in the absence of morphogenesis and to select for putative tubulogenesis process-associated transcripts, essentially subtracting out a background composed of not only noninduced transcripts but also transcripts up-regulated during proliferation. In the heat map set in Fig. 2, it can be seen that the MRSL set of 217 sequences (Table 1; Supplementary Table S2)

DOI:10.1158/0008-5472.CAN-05-3294

Table 1. Transcript levels for representative MEDIC angiogenesis genes and MRSL genes

	Genbank accession no.	Function category	Normalized increase during proliferation	Normalized increase during tubulogenesis	Full-length gene name
MEDIC genes					
VEGFA	AW473981	ST	1.2	**2.2**	Vascular endothelial growth factor A
VEGFB	U3368	ST	1.3	1.3	Vascular endothelial growth factor B
VEGFD	NM_004469	ST	1.3	1.7	Vascular endothelial growth factor D
FGF1	X59065	CFD/M	1.3	1.2	Fibroblast growth factor (acidic)
FGF2	NM_002006	CFD/M	1.2	1.6	Fibroblast growth factor (basic)
PDGFA	AV729452	CFD/M	1.4	1.1	Platelet-derived growth factor-α/ECGF-1
LeptinR	U66496	ST	1.3	1.5	Leptin receptor
SDF1	AL137026	M/CT	1.3	1.7	Stromal cell–derived factor 1/CXCL12
Endothelin-1	S56805	ST	1.7	1.4	Endothelin-1
TF	AI085165	ST	**2.3**	**2.5**	Coagulation factor III/thromboplastin/ tissue factor/CD142
Tie2	XM_005480	ST	**3.2**	1.2	TEK tyrosine kinase, endothelial
EphB4	NM_004444	ST	1.1	1.4	EPH-like receptor protein tyrosine kinase B4
Neuropilin 1	AF145712	ST	1.7	1	Neuropilin 1
αV	XM_002379	M/CT	1.1	1.3	Integrin α_V (vitronectin receptor CD51)
VCAM1	NM_001078	CA	1.3	1.7	Vascular cell adhesion molecule-1
MMP1	M13509	P/MMP	1	1.4	Matrix metalloproteinase-1 (interstitial collagenase)
MMP7	X07819	P/MMP	1.2	1.1	Matrix metalloproteinase-7 (matrilysin, uterine)
MMP9	NM_004994	P/MMP	1.1	1.3	Matrix metalloproteinase-9 (gelatinase B)
Rac1	XM_016309	CSO	1.1	1.2	Small GTP-binding protein Rac1
RhoA	L25080	CSO	1.1	1.4	GTP-binding protein RhoA
COX2	D28235	M/CT	1.6	1.7	Prostaglandin-endoperoxide synthase 2
HIF1A	AI559451	H/TF	1	1.3	Hypoxia-inducible factor 1, α subunit
NFKB 2 p49/p100	NM_002502	H/TF	1.5	1.6	Nuclear factor of κ light polypeptide
Early MRSL transcripts					
**ADA*	NM_000022	AF/GC	1	**4.9**	Adenosine deaminase
**SLIT2*	NM_004787	AF/GC	0.9	**2.4**	Slit homologue 2
HXB/tenascin C	NM_002160	CA/M/CT	0.8	**4.3**	Hexabrachion/tenascin C/cytotactin
PKD1	NM_000296	CA	1	**2.2**	Polycystic kidney disease 1
**CLDN7*	NM_001307	CA	0.9	**2**	Claudin 7
SOS1	NM_005633	CSO	1	**4**	Son of sevenless, homologue 1
† *EFNA1*	NM_004428	CSO	0.9	**2.4**	Ephrin A1
EGFR (truncated)	U48722	CFD/M	0.8	**6.7**	Epidermal growth factor receptor, truncated form
COL5A1	AI983428	ECM/CFD/M	0.8	**2.8**	Collagen, type V, α1
**INSR*	AA485908	DEF	0.8	**2.3**	Insulin receptor
* † *SERPINB6*	AW262311	DEF	0.5	**4.5**	Serine protease inhibitor B6
† *GSTM2*	NM_000848.1	DEF	0.7	**1.7**	Glutathione *S*-transferase M2 (muscle)
† *GSTM1*	NM_000561.1	DEF	0.7	**2.2**	Glutathione *S*-transferase M1
† *GSTM3*	AL527430	DEF	0.9	**3.3**	Glutathione *S*-transferase M3 (brain)
DLL4	NM_019074	CFD/M	0.9	**6.1**	Delta-like 4 homologue
UNKL	BG335934	H/TF	1	**4.7**	Unkempt-like
† *PRDM15/ZNF298*	BF058757	H/TF	0.6	**2.3**	Proline-rich domain zinc finger protein 15
POLYCOMB/NSPC1/RNF3A2	BC004952.1	H/TF	1	**4.6**	Polycomb
GAKIN/KIF13B	NM_015254	ICT/S	0.9	**2**	Kinesin-like protein GAKIN
PIM1	M24779	ICT/S	0.9	**2**	Oncogene pim1
† *ARHGEF7/COOL-1/p85*	AW139757	M/CT	0.9	**2.3**	Rho guanine nucleotide exchange factor 7
CDC42BPB	NM_006035	CSO	1	**2.3**	Cdc42-binding protein kinase β
**LPL*	NM_000237	L-MET	0.9	**3.3**	Lipoprotein lipase
SEC14L2	R49343	L-MET	0.7	**2.9**	Sec14-like 2
† *BRUNOL5*	BE503640	RP	1	**2.5**	Bruno (*Drosophila*) like 5
† *ANKRD3/RIP4/DIK*	NM_020639	ST	0.4	**11.6**	Ankyrin repeat domain 3
† *EFNA3*	AW189015	AF/GC	0.9	**4.5**	Ephrin A3

(*Continued on the following page*)

DOI:10.1158/0008-5472.CAN-05-3294

Table 1. Transcript levels for representative MEDIC angiogenesis genes and MRSL genes (Cont'd)

	Genbank accession no.	Function category	Normalized increase during proliferation	Normalized increase during tubulogenesis	Full-length gene name
**EFNB2*	BF001670	AF/GC	1	**3.8**	Ephrin B2
** † CHRNA3*	M37981.1	AF/GC	0.9	**2.1**	Nicotinic acetylcholine receptor A3
**sFRP1/FrzA*	NM_003012.2	AF/GC	0.9	**3**	Secreted Frizzled-related protein 1
† EVA1	BF437750	CA	0.6	**5.1**	Epithelial V-like antigen 1
**GJA4*	M96789	CA	0.9	**3.2**	Connexin 37
† DUSP4	NM_057158	ST	0.9	**7.8**	Dual-specificity phosphatase 4
SSAT	M55580.1	CFD/M	0.9	**1.9**	Spermidine-spermine *N*1-acetyltransferase
**Nestin*	P48681	CSO	0.9	**2.9**	Nestin
† TAGLN/SM22	NM_003186	CSO	0.9	**4.2**	Transgelin
ZCWPW1	NM_017984	H/TF	0.8	**2.2**	Zinc finger, CW-type with PWWP domain 1
nFATc2/nFAT1	NM_012340	H/TF	0.9	**13.4**	Nuclear factor of activated T cells, calcineurin-dependent 2
ABCA1	AF285167	L-MET	0.8	**2.8**	ATP-binding cassette transporter 1
† CYP1A1	NM_000499	L-MET	0.9	**3.8**	Cytochrome *P*450, subfamily 1
**CXCR4*	AJ224869	M/CT	0.5	**16.7**	Chemokine (C-X-C motif), receptor 4
RGS3	NM_017790	M/CT	1	**2.9**	Regulator of G protein signaling 3
ARHGEF17/p164RhoGEF	NM_014786	M/CT	0.9	**2.1**	Rho guanine nucleotide exchange factor 17
CD10	NM_007287.1	P/MMP	0.9	**3**	Neutral endopeptidase, enkephalinase, CALLA, EC3.4.24.11
T3JAM	NM_025228	ST	0.7	**5.7**	Traf3-interacting JNK-activating modulator
† DUSP10	N36770	ST	0.9	**2.2**	Dual-specificity phosphatase 10
PDE3A	NM_000921	ST	1	**4.7**	Phosphodiesterase 3A
Late MRSL transcripts					
**SEMA4B/SEMAC*	NM_020210	AF/GC	0.9	**2**	Semaphorin 4B
SEMA3C/SEMAE	NM_006379	M/CT	0.9	**2.1**	Semaphorin 3C
SEMA4C/SEMAF	AI949392	M/CT	1	**7**	Semaphorin 4C
TGFBI	NM_000358	CA	0.7	**2.8**	Transforming growth factor-β induced
Syndecan-1/CD138	Z48199	CA/CSO	0.8	**2.5**	Syndecan-1
COL18A1	AF018081	CA	1	**2.9**	Collagen, type XVIII, α1
**GPC1*	NM_002081	CA	0.8	**1.9**	Glypican 1
ITGB4/CD104	NM_000213	CA	1	**2.9**	Integrin β_4
DDR1/NTRK4/NEP/trkE	U48705	CA	1	**2.2**	Receptor tyrosine kinase DDR
**TSC22*	AK027071	CFD/M	0.9	**1.8**	TGF-β-stimulated clone 22
IGFBP5	L27560.1	CFD/M	0.8	**7.4**	Insulin-like growth factor binding protein 5
** † SERPINB9/CAP3*	BC002538	DEF	0.8	**2.2**	Serine proteinase inhibitor, clade B, member 9
**CD59/MIRL/Protectin/MIC11*	NM_000611	DEF	0.9	**2.8**	
** † CSPG2/versican*	BF218922	ECM	0.9	**4.8**	Chondroitin sulfate proteoglycan 2
LAMA5	NM_005560	ECM	1	**2.5**	Laminin, α5
KLF15	AW014734	L-MET/H/TF	1	**2.3**	Kruppel-like factor 15
**BCL6/ZFP51/LAZ3*	NM_001706	H/TF	0.9	**1.9**	B-cell lymphoma 6
Twist2/DERMO1	AI086614	H/TF	0.9	**4.2**	Dermis-expressed protein 1, mouse, homologue of
BTEB1/KLF9	NM_001206	H/TF	0.9	**2.4**	Basic transcription element binding protein 1/Kruppel-like factor 9
HMGIY/HMGA1	NM_002131	H/TF	0.9	**2.6**	High-mobility group protein isoforms I and Y
IRF4/LSIRF/MUM1	D78261	H/TF	1	**3.8**	IFN-regulatory factor
† TLE2/ESG2/GROUCHO2	NM_003260.1	H/TF	0.8	**1.7**	Transducin-like enhancer protein 2
**CITED2/MRG1*	AW027167	H/TF	0.9	**2.5**	CBP/p300-interacting transactivator, with Glu/Asp-rich COOH-terminal domain, 2
† MLPH/SLac2a	NM_024101	ICT/S	0.7	**4.5**	Melanophilin

(*Continued on the following page*)

DOI:10.1158/0008-5472.CAN-05-3294

Table 1. Transcript levels for representative MEDIC angiogenesis genes and MRSL genes (Cont'd)

	Genbank accession no.	Function category	Normalized increase during proliferation	Normalized increase during tubulogenesis	Full-length gene name
DCTN2/p50	NM_006400	ICT/S	1	**2.8**	Dynactin 2
**PDLIM1/ELFIN/CLIM1/CLP36*	BC000915	ICT/S	1	**2.2**	PDZ and LIM domain protein 1
MYO10	NM_012334	ICT/S	1	**2.6**	Myosin X
STK35/Clik1	AA001414	M/CT	0.9	**1.9**	Serine/threonine kinase 35
**HK2*	AI761561	MET	0.9	**1.8**	Hexokinase 2
**SLC2A3/GLUT3*	NM_006931.1	MET	0.8	**1.8**	Solute carrier family 2 (glucose transporter), member 3
† *ABCG1*	NM_004915	L-MET	0.9	**2.6**	ATP-binding cassette, subfamily G (white), member 1
PALM	NM_002579	M/CT	0.8	**1.8**	Paralemmin
SPAG6	AI651156	M/CT	0.9	**2**	Sperm-associated antigen 6
MR-GEF/GFR/REPAC	NM_012294	M/CT	1	**2.5**	Guanine nucleotide exchange factor for Rap1/M-Ras-regulated GEF
BCR	NM_004327.2	M/CT	1	**2**	Breakpoint cluster region protein
CDC42EP3/BORG2	AI801777	M/CT	1	**2.9**	Cdc42 effector protein 3
CTSH	NM_004390.1	P/MMP	0.6	**2.4**	Cathepsin H
ADAM19/MADDAM	Y13786.2	P/MMP	0.8	**3.6**	Murine meltrin-β/ADAM 19 homologue

NOTE: A list of transcript levels as determined from microarray data collected and analyzed as described in Materials and Methods. Top: a subset of the 203 genes defined by the MEDIC Breast Cancer Project as being relevant to the angiogenic process; middle: MRSL transcripts induced early during tube formation (i.e., by 1 hour postplating); bottom: MRSL transcripts induced late during tube formation (i.e., between 1 and 4 hours postplating). Each transcript has an associated gene symbol, Genbank accession no., assigned function category (see text for details), and normalized maximum transcript level achieved during proliferation and tubulogenesis under the conditions described in Materials and Methods. An asterisk notates a gene previously associated with tube formation/angiogenesis. A dagger indicates a clustered gene. Numbers in boldface notate increases of expression, which are statistically significant.

reflects very low levels of expression during proliferation yet very high normalized levels during tubulogenesis. The 217 MRSLs should not be construed as the complete module of genes operating during endothelial cell morphogenesis, but the set of genes whose change in expression most completely distinguishes endothelial cell morphogenesis from the more functionally simple endothelial cell proliferation.

Temporal expression profiles were validated using QRT-PCR on 52 target sequences: 44 MRSLs, 2 down-regulated sequences, and 6 sequences expressed during both time series. RNA samples used as templates for this analysis were isolated from multiple independent experiments by multiple investigators to generate a robust set of validated gene expression patterns. A representative data set is shown in Fig. 3. Time points to 4 hours postinduction confirmed the overall expression pattern seen in the microarrays in 42 of 44 (95%) MRSL sequences. In multiple instances, QRT-PCR-derived induction values were significantly higher than predicted from corresponding microarray values (see, for instance, ephrin A1 and REPAC/MR-GEF in Fig. 3) as would be anticipated from a method with a wider dynamic range of detection.

Antibodies to MRSL proteins were used as probes to ascertain the pattern of expression of proteins corresponding to microarray-detected transcripts. All 16 MRSL proteins assayed at 7 to 8 hours postinduction were detectable by immunofluorescent microscopy (Fig. 4; Supplementary Fig. S4). Protein presence was highly correlated to transcript presence, as evidenced by undetectable fluorescence in control proliferating HMVECs for 13 of the antibodies, and the low level of fluorescence detected using the anti-nestin, anti-SLIT2, and anti-GSTM1 antibodies, a pattern matched by their corresponding transcript levels. The temporal relationship between transcript up-regulation and protein expression was examined for the C-type lectin tetranectin. An increase above a normalized expression value of 1.0 for the tetranectin transcript using the microarray data is first detected at 1 hour postinduction with Matrigel during tube formation, with transcript levels peaking at 2 hours postinduction (Fig. 5, *top*). Protein levels lag behind transcript levels as measured by Western blot, attaining maximal levels at 4 hours postinduction (Fig. 5, *bottom*).

Chromosomal localization of the 217 morphogenesis-specific transcripts indicated that MRSL sequences map to all human chromosomes, except Y, with 23 of the 217 genes lying within 2 or 3 genes of at least one other MRSL gene in 200-kb to 1-Mb length regions at 10 different loci. Seven of the 10 cluster sites consist of nonrelated sequences, whereas the other 3 clusters are at least partly composed of tandem clusters of related genes (Table 1, † genes). Distribution of the MRSL genes among the chromosomes appears random, as the correlation coefficient between the number of MRSL genes on a chromosome and the total number of predicted genes on that chromosome approached 1 ($r^2 = 0.78$, 95% confidence interval; Supplementary Fig. S5). However, Monte Carlo simulations of MRSL gene distribution within individual chromosomes indicate that gene clustering by chance is a statistically low probability event (Supplementary Table S3). As an example, the probability of obtaining one of the two MRSL clusters on

DOI:10.1158/0008-5472.CAN-05-3294

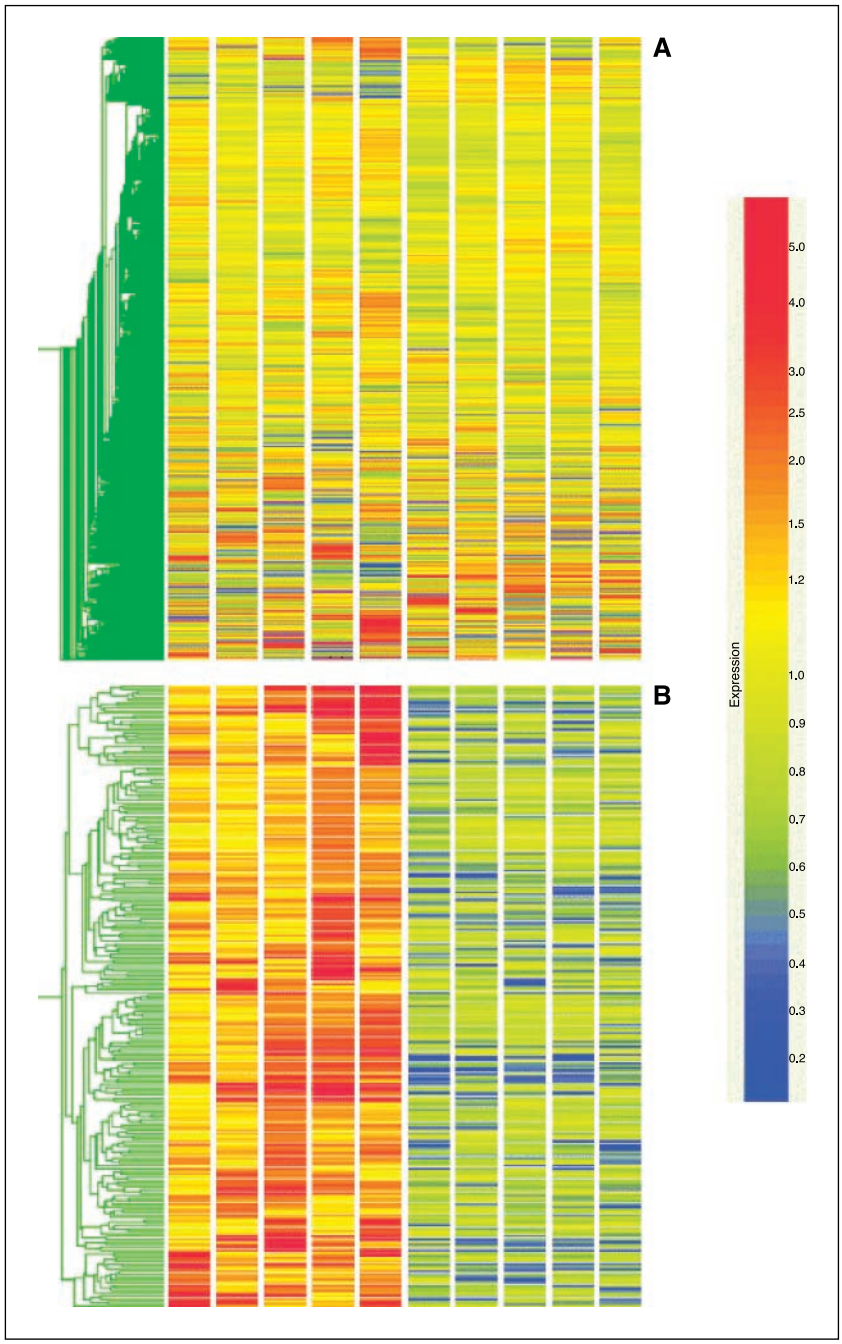

Figure 2. Microarray-based Gene Expression Tree for all chip sequences and derived MRSL sequences. The normalized expression levels for all ≥44,000 (*A*) and all 217 (*B*) MRSL chip sequences at all 10 time points (*columns 1-5,* "tube series" 0.5, 1, 2, 4, and 8 hours; *columns 6-10,* "VEGF series" 0, 0.5, 1, 2, and 4 hours) are depicted with the default color scheme, where the range around 1.0 is yellow, with increasing expression going toward red and decreasing expression going toward blue. Note the dramatic enrichment postfiltration for low-expressing genes during proliferation and highly elevated genes during tubulogenesis.

chromosome 19 by random chance is $0.13 \times 0.13 \times 0.13 = 0.0022$ or 0.22%. Analysis of the temporal expression profiles of genes neighboring the other 194 MRSL genes within ±500 kb with a less stringent mathematical definition of morphogenesis-selective increased the number of identified MRSL gene clusters to a total of 27, including 41 MRSL genes of the original 217.[3]

It has been postulated that large-scale cellular processes, such as differentiation, may require large-scale nuclear reorganization to position the active genes at the surface of chromosome territories and facilitate access to the transcription and splicing machinery (22, 23). This architectural reorganization would be expedited by the clustering along the chromosome of coregulated sequences into "expression neighborhoods" (24). Several MRSL transcripts were found to involve higher-order regulation of gene expression, including the architectural transcription factors polycomb, PRDM15/ZNF298, NSE1, BAZ2A, BCL6, and HMGIY, which modulate chromatin structure (25). The increase seen in levels of proteins associated with chromatin remodeling and the chromosomal clustering of a subset of MRSL genes suggests that a requirement for dynamic colocalization of active genes may be an underlying factor in the regulation of some aspects of endothelial cell morphogenesis.

[3] W. Zhang et al., in preparation.

DOI:10.1158/0008-5472.CAN-05-3294

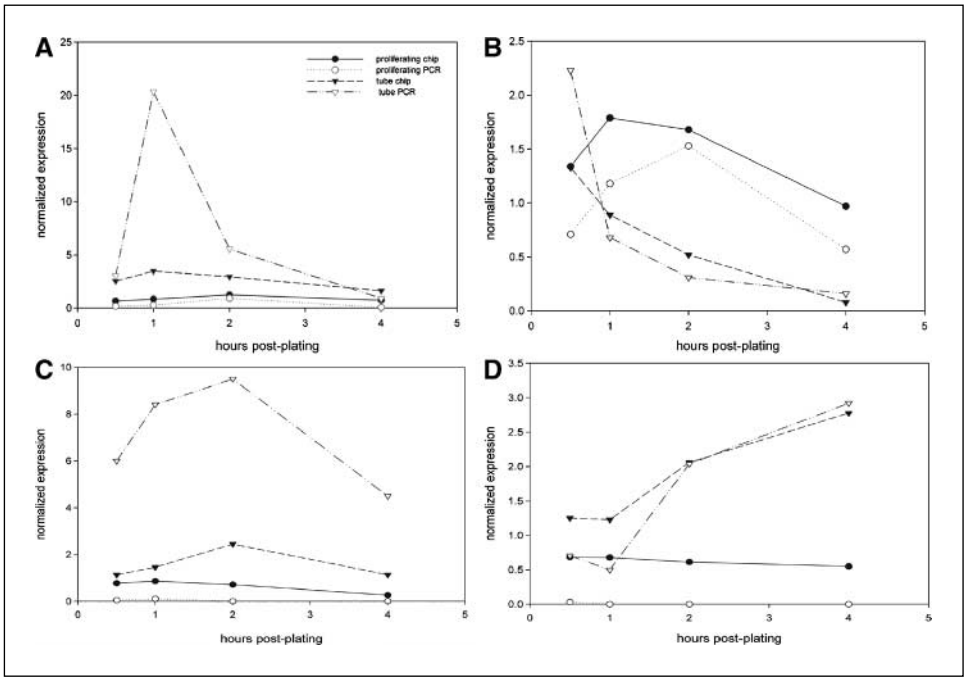

Figure 3. Oligonucleotide array and QRT-PCR of representative transcripts during parallel proliferation and tube formation. A comparison of four representative transcript levels measured with arrays and QRT-PCR. QRT-PCR RNA levels were normalized using rRNA as an internal control. RNA samples were collected out to 4 hours postplating, with proliferating cells plated on plastic measured using arrays (●) or QRT-PCR (○) and tube-forming cells plated on Matrigel using arrays (▼) or QRT-PCR (▽). Ephrin A1 (*A*), REPAC (*C*), and ADAM19/MADDAM (*D*) are all MRSL sequences, whereas Cyr61 (*B*) is down-regulated from its starting level during both time series by 2 hours postplating.

Functional annotation of the 217 MRSL transcripts shows that ~70% of morphogenesis-selective sequences are involved in one of eight functions: regulating gene expression, either as a homeobox or transcription factor protein (H/TF = 17%) followed in order by intracellular trafficking (ICT/S = 10%), motility (M/CT = 9%), cell adhesion (CA = 9%), cell fate determination (CFD/M = 9%), angiogenic factors/guidance cues (AF/GC = 6%), signal transduction (ST = 6%), and cytoskeletal reorganization (CSO = 5%; Table 1; Supplementary Table S2; Supplementary Fig. S6A). Combination of the M/CT and CSO categories to create a larger "cell shape" group resulted in a larger category second in size (14%) only to gene expression regulators. With the exclusion of transcription factors, this translates into 50% of the MRSL products relating to polarity.

Table 1 lists a representative subset of MRSLs in which "early transcripts" refer to initial up-regulation at 30 minutes and 1 hour and "late transcripts" up-regulate at 2 and 4 hours postinduction. The pattern of induction of MRSL transcripts within each function category was analyzed, with representative trends shown in the bar

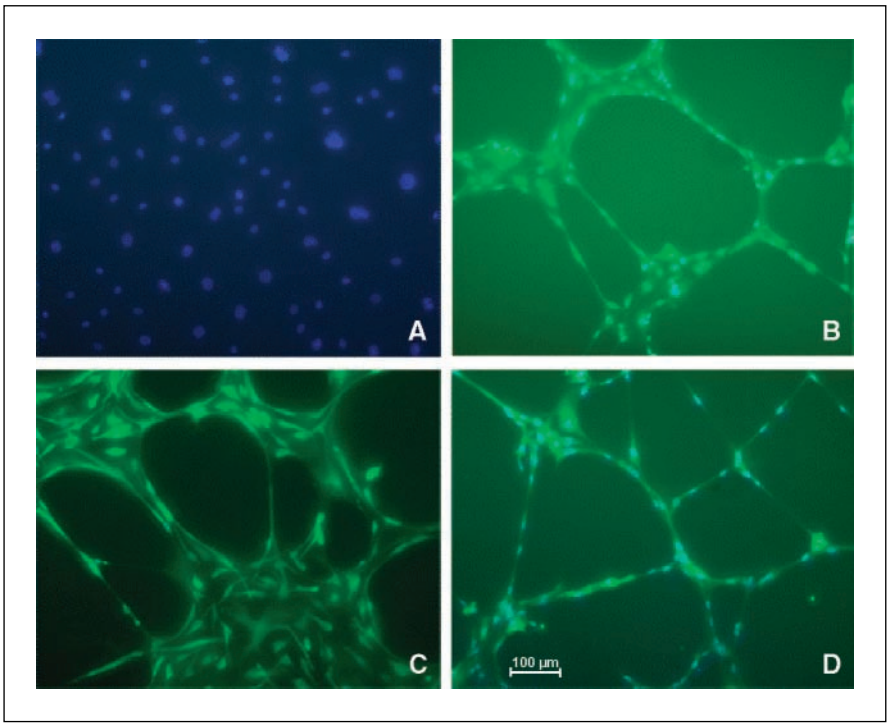

Figure 4. Immunofluorescent analysis of representative MRSL proteins in fixed 8-hour tube structures. Actively proliferating (*A*; representative control) and 8-hour (*B* and *C*) and 7-hour (*D*) formaldehyde-fixed HMVEC tube structures were immunostained with primary antibodies against ephrin A1 (*A* and *B*), nestin (*C*), and ADAM19/MADDAM (*D*), counterstained with Alexa Fluor–labeled secondary antibodies, and visualized at ×100 magnification. Protein was detected in the tube structures for these three antibodies and for antibodies against an additional 13 proteins (Supplementary Fig. S4).

DOI:10.1158/0008-5472.CAN-05-3294

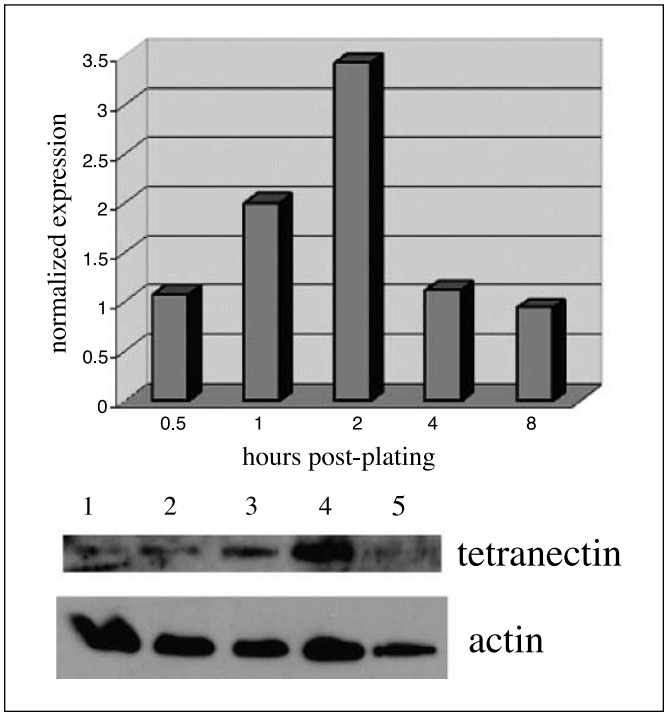

Figure 5. Tetranectin expression during HMVEC tube formation. *Top,* tetranectin transcript levels as measured via array analysis peak at ~2 hours postplating. *Bottom,* a Western blot using anti-tetranectin antibody for 0.5, 1, 2, 4, and 8 hours postplating (*lanes 1-5*) shows that peak tetranectin protein levels lag behind transcript levels, showing maximal levels at 4 hours postplating (*lane 4*). *Bottom,* the same membrane was probed with anti-actin antibody.

graphs in Supplementary Fig. S6B. A large number of functions reflect a phase shift at 2 hours postinduction, with either maximal up-regulation or a second peak of up-regulation occurring at 2 hours postinduction. Further breakdown of the cell fate determining MRSLs showed that 17 of 19 were associated with negative growth control, with cyclin B2 and Est1A being the exceptions and up-regulating early at 30 minutes. This is consistent with the well-known antithetical relationship between proliferation and differentiation in multicellular organisms.

Discussion

Early establishment of cellular polarity is characteristic of tube formation, requiring a major reorientation of the cellular actin cytoskeleton and the formation of abundant actin-based filopodia (Fig. 1*A*; Supplementary Fig. S1A; refs. 10–12). Maintenance of the molecular identity of each of those regions requires intricate sorting and trafficking mechanisms. Consistent with this requirement, 10% of the MRSLs are associated with various aspects of intracellular transport. Components of both the microtubule-based motor complexes (PIM1 and DCTN2 promote dynein/dynactin complex formation; GAKIN/KIF13B is a kinesin-like motor protein) and the actin cytoskeletal motor complexes (MLPH/SLac2a is a cargo adaptor for the actin-based motor protein myosin Va; PDLIM1/ELFIN can localize cargo, such as the MRSL protein STK35 to actin stress fibers) are selectively up-regulated during the tube formation process. It has been shown that microtubule extension occurs preferentially along actin-based filopodia, which act as microtubule polymerization guides in neuronal growth cones, another system that involves the formation of long-range, guided cellular extensions of specialized function (26). It is possible that the motor-related MRSL proteins we have identified may be required to maintain the length of the extended filopodia seen in Fig. 1*A* during initial tube formation.

Up-regulated motility-associated MRSL transcripts appear at an almost constant rate over the first 4 hours of tube formation (Supplementary Fig. S6B), implying an almost constant regulation of motility during the process. These data are in accord with careful studies carried out by Meyer et al. (27) and Connolly et al. (10), indicating that, subsequent to primitive cord-like structure formation, further cell migration occurs by nonnetworked cells through previously made channels in the matrix and by crawling over preexisting tube structures, resulting in a more mature, higher cell density tubule network. Interestingly, the Sprouty-related protein Spred 1 increases over 2-fold between 2 and 4 hours post-Matrigel stimulation, remaining relatively flat during proliferation, implicating this protein in the inhibition of endothelial cell migration postnetwork formation (Supplementary Fig. S7; ref. 28). The majority of M/CT MRSL genes are signal transduction molecules, not architectural proteins, as would be expected from a transcriptome-based analysis. Between 4% and 5% of the MRSL sequences are G protein regulators, including six guanine nucleotide exchange factors and three GTPase-activating proteins (Table 1). These genes reveal molecular footprints for the small GTPases Rho, Rac, Rap, Ras, and Cdc42 as well as the G protein Gα11. Although the mechanisms by which this family regulates actin microfilament dynamics are complex and not fully understood, our identification of numerous members of these families as MRSLs suggests a prominent role for their signaling during endothelial cell tubulogenesis.

MRSL transcripts associated with guidance (AF/GC) and adhesive (CA) properties each exhibit a single peak of maximal up-regulation at 1 and 2 hours, respectively (Supplementary Fig. S6B). Davis et al. (29) observed that endothelial cells release autocrine factors influencing the invasive properties of nearby endothelial cells, with the use of axon guidance transcripts, such as MRSLs SLIT2, the Semaphorins, and the ephrins as mediators of tissue morphogenesis having been noted by many others (30). The continued up-regulation of angiogenic and guidance factors throughout most of this process suggests that endothelial cells require constant molecular feedback to construct proper tubule structures. The large number of adhesion-modulating molecules produced during tubulogenesis may reflect the fact that changing patterns of surface chemistry are central to the rearrangement of cellular assemblies (31), with lumen formation being a simple consequence of differential adhesion in cells expressing adhesive properties in a polarized fashion (32). Continual trafficking of cadherins (33, 34) and integrins (35) in the regulation of adherens junction adhesiveness and cell motility, respectively, has been documented. A need for continual modulation of cell surface properties, such as adhesiveness, may be a factor in the large number of MRSL transcripts identified as being associated with trafficking.

The small number of proteases noted in the MRSL list (CD10/CALLA, ADAM19/MADDAM, and cathepsin H) may be involved in the exposure of matricryptic sites within the matrix and modulating adhesive and migratory properties. This could be a factor in the ability of "succeeding" endothelial cells to move through the matrix pathway established by "pioneer" endothelial cells via the creation of a molecular trail of attractants. Surprisingly, multiple matrix metalloproteinases (MMP) are up-regulated by proliferating endothelial cells unstimulated by matrix material (such as high levels of MMP2, MMP14, MMP19, and MMP24; data

DOI:10.1158/0008-5472.CAN-05-3294

not shown) as well as by tube-forming cells. An early and continuing up-regulation of transcripts associated with lipid metabolism (L-MET), such as ABCG1, ABCA1, and SEC14L2, can also be seen in the MRSL sequences (Supplementary Fig. S6B). Work by Gerritsen et al. (18) showed a similar up-regulation of lipid metabolism genes at this stage and pointed out a requirement for lipid biosynthesis in vacuole/lumen formation.

These data indicate that, at the transcript level, what most distinguishes *in vitro* endothelial cell tubulogenesis from proliferation is a set of highly choreographed actions of genes and gene products that modulate subcellular localization of cellular and surface components, resulting in higher-order tissue architecture. Expression of these genes is driven by cell/extracellular matrix (ECM) contacts. This work elaborates, at the molecular level, the origin of the biphasic nature of *in vitro* endothelial cell morphogenesis described in the elegant morphologic studies of Connolly et al. (10). Tube formation in artificial matrices is characterized by a rapid onset, long-range, guided migratory phase resulting in a primitive cellular network followed by a longer consolidation/maturation phase involving short-range migration and lumen formation. The novel morphogenetic genes identified herein can be divided into two broad categories: the one-sixth of the genes that modulate gene expression (H/TF) and the majority of the remaining genes that generate or maintain polarity (ICT/S, CSO, AF/GC, CA, ECM, and P/MMP).

This analysis further shows that few of the molecular targets of angiopreventive drugs in development are specific to endothelial cell morphogenesis, as most were found to be up-regulated at high levels in proliferating endothelial cells not undergoing tube formation. The 217 human proteins identified in this simple *in vitro* system provide initial information about the kinds of proteins that are involved with such processes as shape change, polarization, and guided migration. The identification of protein targets expressed early within the *in vitro* process and associated with the morphogenesis component of tube formation may, subsequent to follow-up *in vivo* studies, eventually provide better targets for pharmacologic intervention, which can interfere in multiple aspects of aberrant capillary growth associated with numerous human disorders.

Although previous efforts have been made to molecularly dissect the individual components of multicomponent processes (e.g., ref. 36), none have taken this type of high-throughput systems biology approach coupling microenvironmental manipulation of cells with a rigorous analysis of subtracted temporal gene expression "patterns." Our subtractive analysis of transcriptome transformation over time has identified moderately expressed genes up-regulated in the tube-forming cells that are not observed during undirected proliferation. This novel systems biology approach is a generally applicable tool for the molecular dissection of complex biological processes and has the potential to contribute information not readily available by other experimental means.

Acknowledgments

Received 9/14/2005; revised 1/27/2006; accepted 2/20/2006.

Grant support: U.S. Department of Energy contract W-31-100-Eng-38.

The costs of publication of this article were defrayed in part by the payment of page charges. This article must therefore be hereby marked *advertisement* in accordance with 18 U.S.C. Section 1734 solely to indicate this fact.

We thank the staff at sector 2, XOR-CAT, at the Advanced Photon Source, Argonne National Laboratory, for the use of the DIC microscope; the assistance and advice of Dr. X. Li at the Functional Genomics Facility and Y. Chen at the Electron Microscopy Center at the University of Chicago and E.C. Uberbacher at ORNL for helpful discussions. All primary microarray data has been deposited in the Gene Expression Omnibus database at the NCBI in MIAME guideline format upon publication under series record number GSE3891.

References

1. Auerbach R, Lewis R, Shinners B, Kubai L, Akhtar N. Angiogenesis assays: a critical overview. Clin Chem 2003;49:32–40.
2. Glienke J, Schmitt AO, Pilarsky C, et al. Differential gene expression by endothelial cells in distinct angiogenic states. Eur J Biochem 2000;267:2820–30.
3. Jih YJ, Lien WH, Tsai WC, Yang GW, Li C, Wu LW. Distinct regulation of genes by bFGF and VEGF-A in endothelial cells. Angiogenesis 2001;4:313–21.
4. Abe M, Sato Y. cDNA microarray analysis of the gene expression profile of VEGF-activated human umbilical vein endothelial cells. Angiogenesis 2001;4:289–98.
5. Grove AD, Prabhu VV, Young BL, et al. Both protein activation and gene expression are involved in early vascular tube formation *in vitro*. Clin Cancer Res 2002;8:3019–26.
6. Gerritsen ME, Soriano R, Yang S, et al. Branching out: a molecular fingerprint of endothelial differentiation into tube-like structures generated by Affymetrix oligonucleotide arrays. Microcirculation 2003;10:63–81.
7. Kubota Y, Kleinman HK, Martin GR, Lawley TJ. Role of laminin and basement membrane in the morphological differentiation of human endothelial cells in capillary-like structures. J Cell Biol 1988;107:1589–98.
8. Wilson MJ, Sinha AA. Human prostate tumor angiogenesis in nude mice: metalloprotease and plasminogen activator activities during tumor growth and neovascularization of subcutaneously injected Matrigel impregnated with human prostate tumor cells. Anat Rec 1997;249:63–73.
9. Jiang Y, Zhang W, Kondo K, et al. Gene expression profiling in a renal cell carcinoma cell line: dissecting VHL and hypoxia-dependent pathways. Mol Cancer Res 2003;1:453–62.
10. Connolly JO, Simpson N, Hewlett L, Hall A. Rac regulates endothelial morphogenesis and capillary assembly. Mol Biol Cell 2002;13:2474–85.
11. Speidel CC. Studies of living nerves. II. Activities of ameboid growth cones, sheath cells, and myelin segments as revealed by prolonged observation of individual nerve fibers in frog tadpoles. Am J Anat 1933;52:1–79.
12. Gerhardt H, Golding M, Fruttiger M, et al. VEGF guides angiogenic sprouting utilizing endothelial tip cell filopodia. J Cell Biol 2003;161:1163–77.
13. Henderson AM, Wang SJ, Taylor AC, Aitkenhead M, Hughes CC. The basic helix-loop-helix transcription factor HESR1 regulates endothelial cell tube formation. J Biol Chem 2001;276:6169–76.
14. Zhong TP, Rosenberg M, Mohideen MA, Weinstein B, Fishman MC. gridlock, an HLH gene required for assembly of the aorta in zebrafish. Science 2000;287:1820–4.
15. Volin MV, Joseph L, Shockley MS, Davies PF. Chemokine receptor CXCR4 expression in endothelium. Biochem Biophys Res Commun 1998;242:46–53.
16. Liu D, Jia H, Holmes DI, Stannard A, Zachary I. Vascular endothelial growth factor-regulated gene expression in endothelial cells: KDR-mediated induction of Egr3 and the related nuclear receptors Nur77, Nurr1, and Nor1. Arterioscler Thromb Vasc Biol 2003;23:2002–7.
17. Bell SE, Mavila A, Salazar R, et al. Differential gene expression during capillary morphogenesis in 3D collagen matrices: regulated expression of genes involved in basement membrane matrix assembly, cell cycle progression, cellular differentiation and G-protein signaling. J Cell Sci 2001;114:2755–73.
18. Gerritsen ME, Tomlinson JE, Zlot C, Ziman M, Hwang S. Using gene expression profiling to identify the molecular basis of the synergistic actions of hepatocyte growth factor and vascular endothelial growth factor in human endothelial cells. Br J Pharmacol 2003;140:595–610.
19. Chi JT, Chang HY, Haraldsen G, et al. Endothelial cell diversity revealed by global expression profiling. Proc Natl Acad Sci U S A 2003;100:10623–8.
20. Wang JL, Liu YH, Lee MC, et al. Identification of tumor angiogenesis-related genes by subtractive hybridization. Microvasc Res 2000;59:394–7.
21. St Croix B, Rago C, Velculescu V, et al. Genes expressed in human tumor endothelium. Science 2000;289:1197–202.
22. Cremer T, Cremer C. Chromosome territories, nuclear architecture and gene regulation in mammalian cells. Nat Rev Genet 2001;2:292–301.
23. Spilianakis CG, Lalioti MD, Town T, Lee GR, Flavell RA. Interchromosomal associations between alternatively expressed loci. Nature 2005;435:637–45.
24. Oliver B, Parisi M, Clark D. Gene expression neighborhoods. J Biol 2002;1:4.
25. West AG, Fraser P. Remote control of gene transcription. Hum Mol Genet 2005;14:R101–11.
26. Schaefer AW, Kabir N, Forscher P. Filopodia and actin arcs guide the assembly and transport of two

DOI:10.1158/0008-5472.CAN-05-3294

populations of microtubules with unique dynamic parameters in neuronal growth cones. J Cell Biol 2002; 158:139–52.
27. Meyer GT, Matthias LJ, Noack L, Vadas MA, Gamble JR. Lumen formation during angiogenesis *in vitro* involves phagocytic activity, formation and secretion of vacuoles, cell death, and capillary tube remodelling by different populations of endothelial cells. Anat Rec 1997; 249:327–40.
28. Miyoshi K, Wakioka T, Nishinakamura H, et al. The Sprouty-related protein, Spred, inhibits cell motility, metastasis, and Rho-mediated actin reorganization. Oncogene 2004;23:5567–76.
29. Davis GE, Black SM, Bayless KJ. Capillary morphogenesis during human endothelial cell invasion of three-dimensional collagen matrices. In Vitro Cell Dev Biol Anim 2000;36:513–9.
30. Hinck L. The versatile roles of "axon guidance" cues in tissue morphogenesis. Dev Cell 2004;7:783–93.
31. Takeichi M, Nakagawa S, Aono S, Usui T, Uemura T. Patterning of cell assemblies regulated by adhesion receptors of the cadherin superfamily. Philos Trans R Soc Lond B Biol Sci 2000;29:885–90.
32. Newman SA, Muller GB. Epigenetic mechanisms of character origination. J Exp Zool 2000;288:304–17.
33. Kamei T, Matozaki T, Sakisaka T, et al. Coendocytosis of cadherin and c-Met coupled to disruption of cell-cell adhesion in MDCK cells-regulation by Rho, Rac and Rab small G proteins. Oncogene 1999;18:6776–84.
34. Le TL, Yap AS, Stow JL. Recycling of E-cadherin: a potential mechanism for regulating cadherin dynamics. J Cell Biol 1999;146:219–32.
35. Ng T, Shima D, Squire A, et al. PKCα regulates β_1 integrin-dependent cell motility through association and control of integrin traffic. EMBO J 1999;18: 3909–23.
36. Bein K, Odell-Fiddler ET, Drinane M. Role of TGF-β1 and JNK signaling in capillary tube patterning. Am J Physiol Cell Physiol 2004;287:C1012–22.